Supporting information:

Nano-structural stiffness measure for soft biomaterials of heterogeneous elasticity

Shu-wen W. Chen[a,b*], *Jean-Marie Teulon*[a], *Harinderbir Kaur*[a], *Christian Godon*[c], *and Jean-Luc Pellequer*[a*]

[a]Univ. Grenoble Alpes, CEA, CNRS, IBS, F-38000 Grenoble, France

[b]Rue Cyprien Jullin, F-38470 Vinay, France.

[c]Aix Marseille Univ, CEA, CNRS, BIAM, F-13108 Saint Paul-Lez-Durance, France

Corresponding authors : Shu-wen W. Chen (cmft551@yahoo.com); Jean-Luc Pellequer (jean-luc.pellequer@ibs.fr)

Computational procedure

1.a. Criteria of being a contact point

Determination of the contact point is the first step for the formation of indentation curve [1]. On a physical view, before reaching the contact point the tip experiences neither force nor force gradient (the first derivative of force) from the material. As a common practice in the study of nanomechanics, the location of the contact point is not pre-determined, it moves with which section of the curve yielding the best fitting results to the mechanical model used. As a consequence, the contact point lost its physical meaning. In this work, we follow the physical fact for determining the contact point, and we do not assume that the study material is necessarily elastically homogeneous.

Before starting with the curve of force (F_d) versus tip-sample separation (z), z being the cantilever-corrected piezo displacement; a small portion (10%) of initial pre-contacting data points are discarded to prevent unacceptable non-flatness and distortions from the baseline. We applied the Savitzky-Golay (SG) filter [2] to alleviate fluctuations of the data series (the smoothing effects can be seen from **Fig**. **S1**). Basically, the SG filter processes a series of data points in a convolution fashion with a matrix of $(n+1) \times (2w+1)$ convolution coefficients, where w is the half size of the smoothing window, n is the degree of the fitting polynomial function and is the highest order for the derivative function. In this work, we used $n = 3$ and $w = 15$ for all the testing systems. The great advantage of using the SG filter is not only to smoothen noisy data but also to simultaneously calculate the derivative functions.

Fig. S1 describes the detail of locating the contact points (z_c's) of all the study systems based on the criteria, $F_d = 0$ and $\partial F_d/\partial z = 0$. For calculations of $\partial F_d/\partial z$, we first used the SG filter to calculate the first derivative with respect to t or enumeration indexes of data points, $\partial F_d/\partial t$ and $\partial d/\partial t$, at each data point, then $\partial F_d/\partial z$ is calculated as $(\partial F_d/\partial t)/(\partial z/\partial t)$, i.e., the ratio of $\partial F_d/\partial t$ to $\partial z/\partial t$.

1.b. Formation of indentation and stiffness-depth curves

Once the contact point was decided, we generated the plot of F_T against Z (the indentation curve) straightforwardly with that $Z = -(z - z_c)$ and $F_T(Z) = F_d(z) - F_d(z_c)$, then the tip effects were removed from the F_T–Z curve [3]. Since $z = z_c$ was chosen as the origin of the F_T–Z curve, $Z_0 = 0$ and $F_T(Z_0) = 0$. Similar to the calculations for $\partial F_d/\partial z$, the curve of F_T-derived stiffness vs. depth was generated by the following steps: 1) calculate $\partial F_T/\partial t$ and $\partial Z/\partial t$ using the SG filter;

2) calculate the ratio of $\partial F_T/\partial t$ to $\partial Z/\partial t$ as the value of $F_T'(\partial F_T/\partial Z)$; 3) smoothen the F_T'-Z curve using a moving average filter.

2. Heterogeneity of elasticity and segmental analysis of stiffness-depth curve

We adopted a stiffness-based approach to identify the regions of different elasticity in the indentation trajectory. Based on Sneddon's model with pyramidal tips, the stiffness-depth curve (F_T' vs. Z) would appear as a series of linear segments joined at breaking points, B_j's. The Z coordinates of B_j's are referred to as generalized contact points that interface two adjacent depth-zones of different elastic properties. The following describes how linear segments delimiting the depth-zones of different elastic properties are determined from the stiffness-depth curve.

The segmentation of stiffness-depth curve was performed using clusterwise linear regression with the minimal distance method [4]. For a curve consisting of m linear segments, the clusterwise linear regression optimizes all the segments simultaneously with $2m$ fitting parameters. Subsequently, consecutive points were re-grouped from a cluster and an initial set of linear segments was established. Linearity of two consecutive segments was tested by their intersection angle. If the angle was within 5°, then the two segments were merged together to become one. Each segment required at least $(2w+1)$ data points. For a stiffness segment corresponding to, say Zone j, it has a generic form of a linear function: $c_j + R_{S,j}\times Z$ with c_j and $R_{S,j}$ two fitting parameters. The two parameters are exploited for decomposing F_T into F_C, F_H and F_S.

3. Force decomposition for the trimechanic theory

As F_H component of Zone j is formulated as $k_{\mathrm{H},j}\times(Z-Z_{j-1})$, $k_{\mathrm{H},j} = c_j + R_{S,j}\times Z_{j-1}$ and equals $F_T'(Z_{j-1})$ in Eq. (4). More important, the heterogeneity of material elasticity in the indentation trajectory is differentiated by $R_{S,j}$. F_C is set to $F_T(Z_{j-1})$, whereas the F_S component is the total force F_T subtracting the sum of F_C and F_H. In general, F_C and F_H do not need a fitting function, only F_S needs one. For example, F_S will fit to a parabolic function when a cone-like or pyramidal tip is in use: $f_{p,j}(Z - Z_{j\text{-}1})^2 + \delta_j$, where $f_{p,j}$ and δ_j are two fitting parameters. The effective Young's modulus can be deduced as $\hat{E}_j = \sqrt{2}\, f_{p,j}/tan(\alpha)$ (cf. Eq. (2)) by ignoring the contribution attributed to the modulus of indenting tip itself. The weight of F_S contribution w_S is defined as $F_S(Z_j)/F_T(Z_j)$ to decide whether F_S to be neglected. If $w_S < 0.1$, then F_S is set to zero. Its data values are joined to F_H and the resultant F_H will be re-fitted to $k_{\mathrm{H},j}\times(Z - Z_{j\text{-}1})$, where $k_{\mathrm{H},j}$ now is a fitting parameter instead of an analytical quantity. Consequently, the fitted F_T data values, as presented in **Fig**. **2** and **3**, are the sum of the fitted force and, at most, two other non-fitted ones.

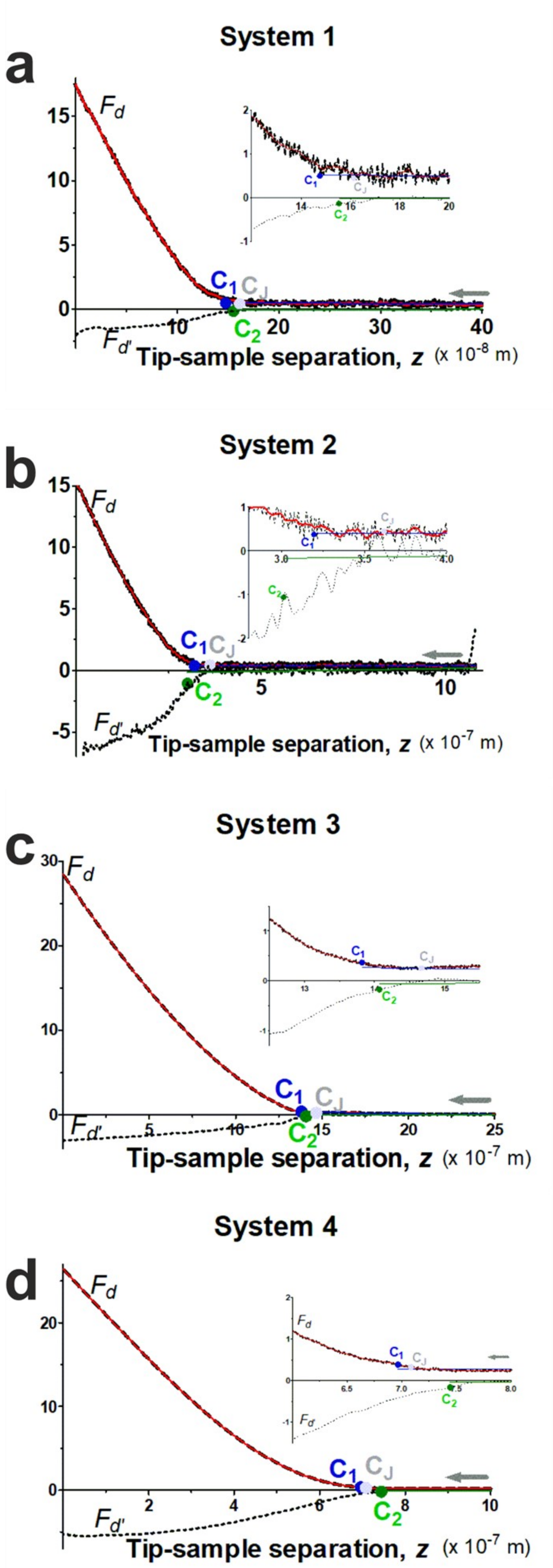
System 1
a
F_d
$F_{d'}$
C_1
C_J
C_2
Tip-sample separation, z (x 10-8 m)
System 2
b
F_d
$F_{d'}$
C_1
C_J
C_2
Tip-sample separation, z (x 10-7 m)
System 3
c
F_d
$F_{d'}$
C_1
C_J
C_2
Tip-sample separation, z (x 10-7 m)
System 4
d
F_d
$F_{d'}$
C_1
C_J
C_2
Tip-sample separation, z (x 10-7 m)

Figure S1: Contact points of all the illustrating systems. The determination of contact point is based on the criteria: $F_d(z) = 0$ and $F_d'(z)=0$ (see the main text). The plots of deflection force, $F_d(z)$, and $F_d'(z)$ have been smoothened by the SG filter beforehand and presented by black dashed lines in the figure. Inset graphs illustrate the smoothing effects of the SG filter. Red lines represent smoothed data of $F_d(z)$. The gray arrow along the z coordinate indicates the approaching direction of the tip toward the material surface. The blue and green lines are the baselines obtained by clusterwise linear regression respective to $F_d(z)$ and $F_d'(z)$. Correspondingly, blue and green spots mark the potential contact points along the $F_d(z)$ and $F_d'(z)$ baselines, and denoted by $\mathbf{C_1}$ and $\mathbf{C_2}$. For comparison, gray spots mark the contact point determined by the AtomicJ-pyramid algorithm, and labeled with $\mathbf{C_J}$. In practice, $\mathbf{C_1}$ and $\mathbf{C_2}$ were chosen as close as possible toward the material surface, where $F_d(z_1)$ and $F_d'(z_2)$ are within, 2.5 for gels and 2.9 for plant roots, standard deviations relative to the respective baselines. From our experience, $F_d'(z)$ is better to reflect the tendency of $F_d(z)$ than $F_d(z)$ itself. Consequently, z_2 is taken as the final location of the contact point. The units of F_d and F_d' are in 10^{-7} m, 10^{-8} N, and 10^{-3} N/m, respectively. (**a**) The hard gel (System 1): $z_1 = 14.9$, $z_2 = 14.9$, and $z_J = 16.1$ ($\times 10^{-8}$ m); F_d and F_d' are in 10^{-10} N, and 10^{-2} N/m. (**b**) The soft gel (System 2): $z_1 = 3.19$, $z_2 = 3.01$, and $z_J = 3.62$ ($\times 10^{-7}$ m); F_d and F_d' are in 10^{-10} N and 10^{-3} N/m. (**c**) The plant root of System 3: $z_1 = 13.8$, $z_2 = 14.1$ and $z_J = 14.68$ ($\times 10^{-7}$ m); F_d and F_d' are in 10^{-9} N and 10^{-2} N/m. (**d**) The plant root of System 4: $z_1 = 6.97$, $z_2 = 7.44$ and $z_J = 7.09$ ($\times 10^{-7}$ m); F_d and F_d' are in 10^{-9} N and 10^{-2} N/m.

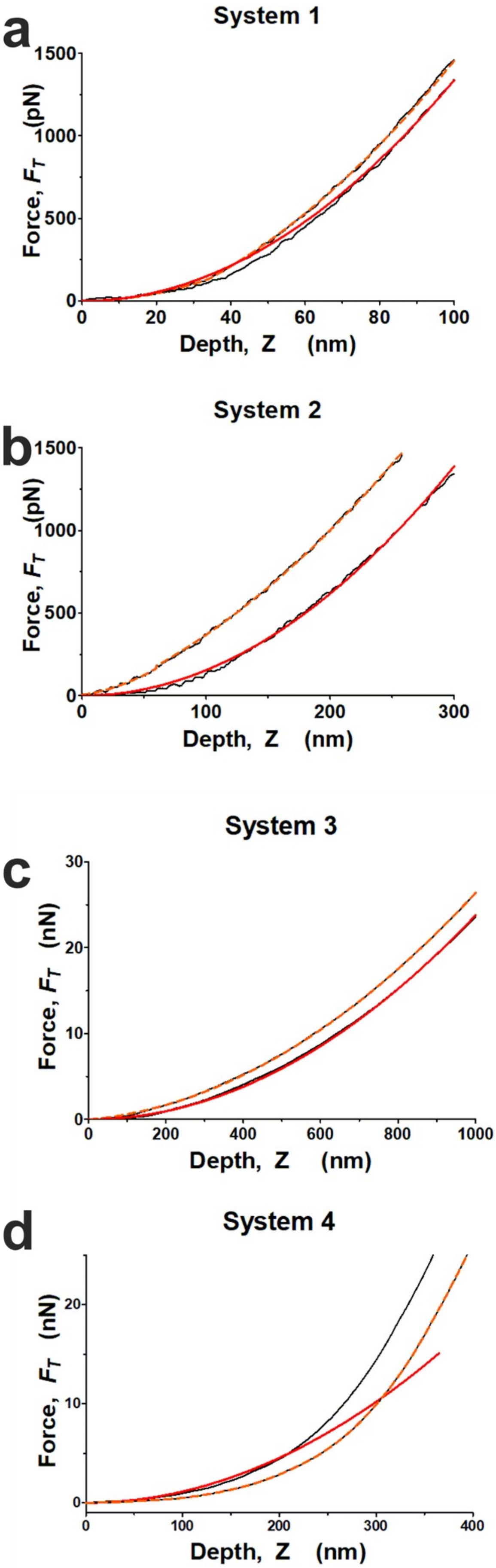
a
System 1
Force, F_T (pN)
Depth, Z (nm)
b
System 2
Force, F_T (pN)
Depth, Z (nm)
c
System 3
Force, F_T (nN)
Depth, Z (nm)
d
System 4
Force, F_T (nN)
Depth, Z (nm)

Figure S2: The fitting results of responding force from AtomicJ-pyramid and the trimechanic-3PCS models. The pyramid model of AtomicJ uses the conventional approach to fitting the responding force where the initial contact point is sought for improving the goodness of the fitting by a robust exhaustive method, LTA [5]. In the parameter setup of AtomicJ, the same semi-vertical angle of the pyramidal tip, 35˚, and a Poisson ratio of 0.0 were used for best comparison with the tri-mechanic-3PCS model to illustrate different consequences from the conventional usage of the Sneddon's model and our strategy. Derived indentation curves from AFM measurements are drawn by thin black lines for both models and the fittings by AtomicJ-pyramid are shown in red whereas that of the trimechanic-3PCS model are in orange dashed lines. (**a**) System 1: the hard gel. AtomicJ-pyramid provides a value of 256 kPa for the effective Young's modulus, equivalent to a stiffness measure of 14.4 mN/m using an indentation transition of 113 nm (see Eq. 5), while our model obtains 230 and 236 kPa for Zone 1 and 2, and the corresponding k_S equals 3.91 and 20.0 mN/m, respectively. (**b**) System 2: the soft gel. The effective Young's modulus deduced from AtomiJ-pyramid is 29.5 kPa, equivalent to a stiffness of 4.37 mN/m at indentation depth of 298 nm. From the trimechanic-3PCS framework, we observed that Ê1 = 54.4 and Ê2 = 23.4 kPa with $k_{S,1}$ = 2.66 and $k_{S,2}$ = 6.52 mN/m, respectively. (**c**) System 3, only one value of effective Young's modulus was deduced from both methods, 45.5 kPa from AtomicJ-pyramid and 45.2 kPa from the trimechanic-3PCS model. (**d**) System 4, AtomicJ-pyramid yields Ê = 214 kPa, while the trimechanic-3PCS model reports five Ê values attributed to the five force/stiffness segments, ranging from 67.5 to 611 kPa (see **Fig. 3**). From the fitting results, one can see by adopting the conventional strategy for stiffness measure, AtomicJ-pyramid displays a poor fitting to the response of material in the initial indentation which is essential for accurately describing the elastic properties of material surface. Ê = 214 kPa from AtomicJ-pyramid is too high to account for the response of material in the initial indentation while it is too low to describe the impact of deepened depth brought on the stiffness magnitude for a material of heterogeneous elasticity.

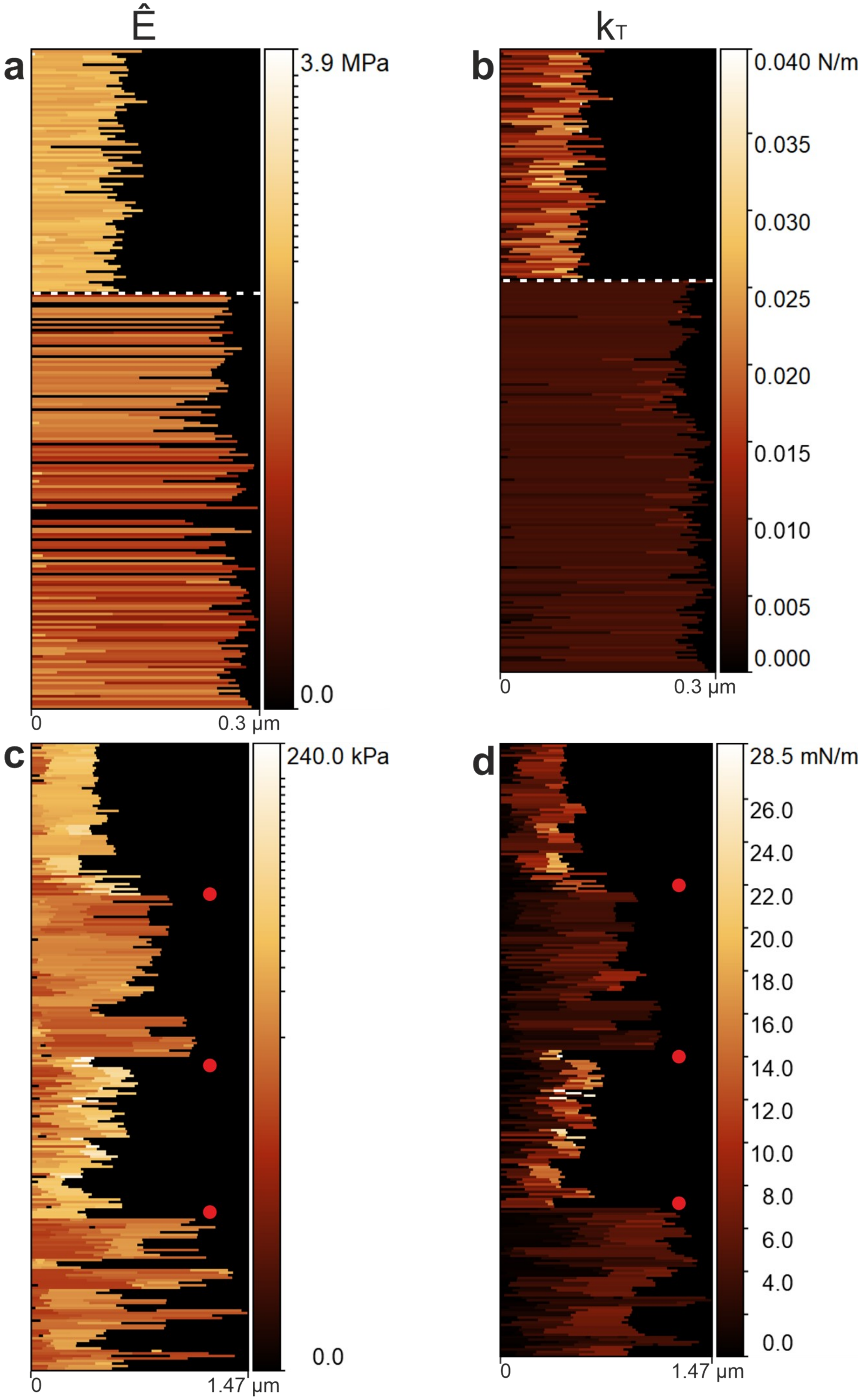

Ê
kT
a
3.9 MPa
0.0
0
0.3 µm
b
0.040 N/m
0.035
0.030
0.025
0.020
0.015
0.010
0.005
0.000
0
0.3 µm
c
240.0 kPa
0.0
0
1.47 µm
d
28.5 mN/m
26.0
24.0
22.0
20.0
18.0
16.0
14.0
12.0
10.0
8.0
6.0
4.0
0.0
0
1.47 µm

Figure S3: Bar graphs of effective Young's modulus and the stiffness measure k_T for polyacrylamide gels and plant roots. The horizontal-axis corresponds to the indented depth; the results of each indentation curve are represented with one line. The color bar on the right of the graph displays the value in the measured quantities. The graphics were generated using the Gwyddion software [6]. (**a**, **b**) The values of $\hat{E}$ and k_T of 91 sampled indentations for the hard gel as prepared for System 1, and beneath are 155 measurements for the soft gel for System 2. The separation of the two groups is marked by white dotted lines. By the naked eye, one can observed that the colors of $\hat{E}$ and k_T for the hard gel are much brighter than for the soft gel. Take the first depth-zone as an example, $\hat{E}_{\mathbf{hard}} = 2.96 \pm 4.02$ MPa (median = 2.27 MPa) vs. $\hat{E}_{\mathbf{soft}} = 0.41 \pm 0.62$ MPa (median = 0.32 MPa); $k_{T,\mathbf{hard}} = 9.96 \pm 4.90$ mN/m (median = 9.68 mN/m) vs. $k_{T,\mathbf{soft}} = 5.02 \pm 1.33$ mN/m (median = 5.51 mN/m). As for the first depth-zone, large standard deviations are observed for all depth-zones and underlie heterogeneity of cross-linker arrangement and inter-subgroup bonding properties. (**c**, **d**) The results of $\hat{E}$ and k_T of 248 indentation experiments on four different plant roots, maximum 64 curves for each root. The red spots mark the separation between the measurements on each roots. We observed that the values of $\hat{E}$, k_T and indentation length fluctuate widely, yet they vary more homogeneously within the same plant root. Recall that these root tissues are living organisms, their physiological conditions continuously change, e.g. the growth rate. For the first depth-zone, the averaged $\hat{E} = 94.9 \pm 101$ kPa with a median value of 58.4 kPa, and $k_T = 12.3 \pm 17.8$ with the median of 4.1 (in mN/m).

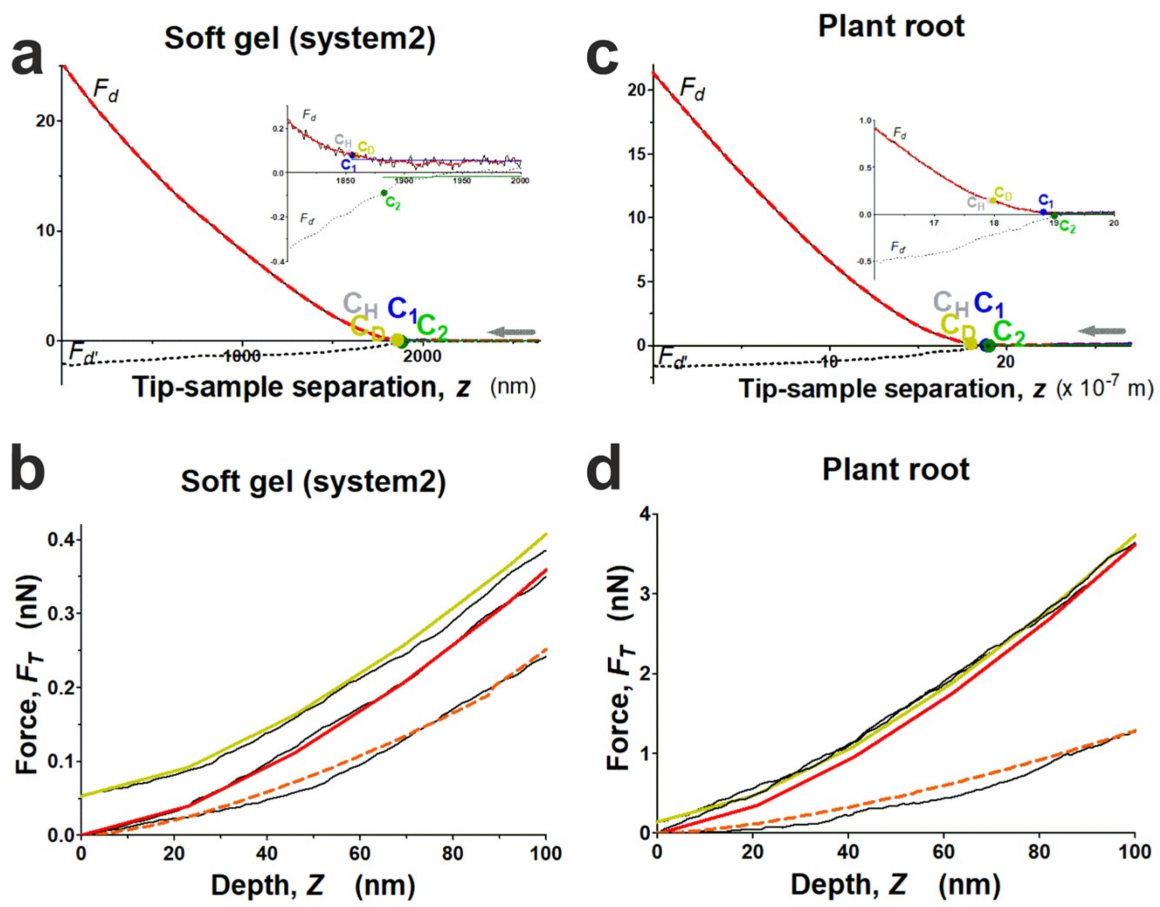

Figure S4: Preliminary test for the trimechanic-3PCS model applied to force-depth curves using a small spherical probe with a radius of 100 nm. The results from the present model are compared with other contact-based models. Locations of the contact points and the fittings of a F_T–Z curve from a soft gel sample **(a,b)** and that on a plant root **(c,d)**. The results from classical paraboloid Hertz and DMT models were obtained using AtomicJ robust exhaustive method, LTA [5] (JKR model from AtomicJ is not shown for lack of successful fitting). Parameter setup of AtomicJ includes the radius of the spherical probe, 0.1 μm, a Poisson ratio of 0, and the data smoothing by the SG filter (w = 10, n = 3). **(a)** Determination of the contact point for the soft gel. $\mathbf{C_1}$ and $\mathbf{C_2}$ mark the potential contact points obtained from $F_d(z)$ and $F_d'(z)$ baselines (cf. **Fig. S1**), whereas $\mathbf{C_H}$ and $\mathbf{C_D}$ mark the contact points identified by the Hertz and DMT models using AtomicJ. Inset graphs show a zoomed area around the contact points. **b)** Comparison of fitting results to individual indentation curves from respective models (thin black lines) within the first 100 nm of indentation depth. Fittings by AtomicJ-Hertz and AtomicJ-DMT are shown in red and olive, respectively, whereas that of the trimechanic-3PCS model are in orange. The effective Young's moduli deduced from AtomicJ-Hertz and AtomicJ-DMT are 26.8 and 26.6

kPa, respectively (both models consider the entire curve as one depth-zone). The trimechanic-3PCS framework yields $\hat{E}1 = 17.3$ and $\hat{E}2 = 21.0$ kPa for two depth-zones. **(c**,**d)** same descriptions as **(a**,**b)** except the system is a plant root. The effective Young's moduli from AtomicJ-Hertz and AtomicJ-DMT are respectively 272 and 270 kPa, while from the trimechanic-3PCS framework, $\hat{E}1 = 96.2$ in the depth range considered. For this case, the greater difference in comparison of Young's moduli is attributed to the large discrepancy in the determined location for the contact point.

References

1. S. L. Crick and F. C. Yin, *Biomech. Model. Mechanobiol.*, 2007, **6**, 199-210.
2. A. Savitzky and M. J. E. Golay, *Anal. Chem.*, 1964, **36**, 1627-1639.
3. P. Carl and H. Schillers, *Pflugers Archiv.*, 2008, **457**, 551-559.
4. H. Spath, *Cluster dissection and analysis theory, fortran programs, examples*, Ellis Horwood Limited, Chichester, 1985.
5. P. Hermanowicz, M. Sarna, K. Burda and H. Gabrys, *Rev. Sci. Instrum.*, 2014, **85**, 063703.
6. D. Nečas and P. Klapetek, *Cent. Eur. J. Phys.*, 2012, **10**, 181-188.